Chemical stability and superconductivity in Ag-sheathed $CaKFe_4As_4$ superconducting tapes

Zhe Cheng,[1,2] Chiheng Dong,[1] He Huang,[1,2] Shifa Liu,[1,2] Yanchang Zhu,[1,2] Dongliang Wang,[1] Vitalii Vlasko-Vlasov,[3] Ulrich Welp,[3] Wai–Kwong Kwok,[3] Yanwei Ma[1,2]

[1] *Key Laboratory of Applied Superconductivity, Institute of Electrical Engineering, Chinese Academy of Sciences, Beijing 100190, China*
[2] *University of Chinese Academy of Science, Beijing, 100049, China*
[3] *Argonne National Laboratory, 9700 South Cass Avenue, Argonne, Illinois 60439, USA*

Abstract

Ag-sheathed $CaKFe_4As_4$ superconducting tapes have been fabricated via the ex situ powder-intube method. X-ray diffraction analyses suggest that the $CaKFe_4As_4$ phase reacts strongly with the silver sheath at temperature above 500 ° C. We therefore anneal the tape at 500 ° C and obtain a transport critical current density J_c (4.2 K, 0 T) ~2.7 x 10^4 A/cm^2 . The pinning potential derived from magnetoresistance measurements is one order of magnitude lower than that of the $(Ba/Sr)_{1-x}K_xFe_2As_2$ tapes. Combining with the scanning electron microscopy and magnetooptical imaging results, we suggest that bad connectivity between superconducting grains caused by the low sintering temperature is the main factor responsible for the low J_c . However, this system is still a promising candidate for superconducting wires and tapes if we find a compatible sheath material and further optimize the post-annealing process to achieve better grain connectivity.

Introduction

The iron-based superconductors (IBSs) are of great interest from a basic point of view as well as in light of practical application [1]. In spite of the large varieties of IBSs with different crystal structures discovered so far, vortex pinning and anisotropy place fundamental restrictions on the current carrying ability. Furthermore, the high field performance of iron-based superconducting wires and tapes fabricated by the powder-in-tube (PIT) method [2] depends on other extrinsic factors, i.e. the purity of the precursors, the compatibility to the sheath material, the density and texture of the superconducting core, and particularly, the homogeneity of the superconducting phase. After ten years of research and design, the optimally doped $(Ba/Sr)_{1-x}K_xFe_2As_2$ has emerged as the

dominant material used in iron-based superconducting wires and tapes. On one hand, the quality of the $(Ba/Sr)_{1-x}K_xFe_2As_2$ precursor has progressively improved due to mature synthesis processes [3] . On the other hand, plenty of technologies, including flat rolling [4 , 5] , cold [6 , 7] and hot [8] uniaxial pressing, hot isotropic pressing [9–11] , as well as double sheath architecture [12] have been applied in the manufacturing process to enhance the texture and density of the superconducting core. Based on these efforts, the critical current density J_c of the $(Ba/Sr)_{1-x}K_xFe_2As_2$ superconducting tapes at 4.2 K and 10 T has been gradually improved and now surpasses the level needed for practical applications [13]. Nevertheless, like other doped IBSs, the superconductivity of the BaK122 system is compromised by the non-uniformly distributed K atoms [14] . The inherent potassium clustering causes an inhomogeneous Jc distribution due to its sensitivity to K content [15]. It deteriorates the overall current carrying capability of the iron-based superconducting wires and tapes, especially at long lengths. Consequently, finding a non-doped, stoichiometric IBS becomes vitally important for practical applications.

The recently discovered $CaKFe_4As_4$superconductor is prominent among stoichiometric IBSs owing to its high superconducting transition temperature of Tc∼35 K [16] which is competitive with the optimally K-doped FeAs122 system. In contrast to the $(Ca_{0.5}\ Na_{0.5})Fe_2As_2$ solid solution with I4/mmm space group, $CaKFe_4As_4$ possesses a P 4/mmm structure with the Ca and K layers alternately stacked between the Fe_2As_2 layers. Potassium doping on the alkaline-earth element site unavoidably introduces substantial disorders. Whereas $CaKFe_4As_4$ is structurally ordered with Ca and K occupying different layers. In addition, there is no structural or magnetic phase transition [17 , 18] , so one could consider this system as an optimally-doped ordered system. The upper critical field B_{c2} of the $CaKFe_4As_4$ singe crystal is 71 T with the field parallel to the c axis and 92 T for the field perpendicular to the c axis [17] . The anisotropy parameter γ below 30 K is less than 2. The depairing current density J_0 at 0 K, estimated from $J_0 = \frac{\Phi_0}{3\sqrt{3}\mu_0\pi\xi\lambda^2}$ is 265 MA cm^{-2} , where Φ_0 is the flux quantum, ξ= 2.15 nm is the coherence length, λ= 133 nm is the penetration depth [19] . This J0 value is even larger than seen in other FeAs122 superconductors [20] . Further magnetic measurements on $CaKFe_4As_4$ single crystals indicate that the critical current density J_c at 10 T is nearly 1MA cm−2 with the field parallel to the c axis [21] . Moreover, it exhibits a more robust temperature dependence than the BaK122 counterpart, making it very promising to be used not only at liquid helium temperature, but also at intermediate temperatures accessible with cryocoolers.

In this paper, we synthesize the CaKFe4 As4 precursor with a two-step method. We find that the superconducting core of the $CaKFe_4As_4$ PIT tape reacts strongly with the Ag sheath during the post-annealing at temperature above 500 °C. Therefore, we sinter the tape at 500 °C and achieve a J_c of 22.7 × 10^4 A/cm^2 at 4.2 K and self-field. We demonstrate that bad connectivity between superconducting grains due to low temperature sintering limits the overall critical current and indicates the need for a well-controlled postannealing method to achieve better connectivity in this system.

Experimental details

In order to improve the homogeneity, we synthesized the precursor according to a two-step method [3] . We firstly prepared the intermediate compounds with nominal compositions CaAs and KAs at 700 °C and 400 °C, respectively. These intermediates were then mixed with Fe powders and As pieces according to the nominal composition $Ca_{1.15}K_{1.05}Fe_4As_4$. Excess CaAs and KAs were added to compensate for the loss of K and Ca during the heat treatment. The mixtures were ball milled for 10 h in Ar atmosphere, sealed in a Nb tube afterwards and directly inserted into a preheated furnace at 900 °C. After 30 h of sintering, the Nb tube was quenched to room temperature [16] . Considering the strong reaction between Cu/ Fe and iron pnictides, we chose Ag as the outer sheath material. After grinding the $CaKFe_4As_4$ precursor into powders, we loaded them into a silver tube with outer and inner diameters of 8mm and 5mm, respectively. The tube was swaged, drawn and rolled into a 0.4mm thick tape. We cut the tape into short samples and finally annealed them at temperatures between 500 ° C and 800 ° C.

The x-ray diffraction (XRD) patterns of the precursors and the tapes were performed on a Bruker D8 Advance x-ray diffractometer. We analyzed the diffraction patterns by Rietveld refinement. The thermogravimetric (TG) and differential thermal analyses (DTA) were performed on a synchronous thermal analyzer (Netzsch; STA 499 F3) at a heating rate of 20 °C min^{-1} . The average composition of the superconducting core is determined by an electron probe micro-analyzer (EPMA) . The transport critical current Ic was measured at 4.2 K via a four-probe method with a criterion of 1 μV cm^{-1} at the High Magnetic Field Laboratory (CHMFL, Hefei) . We measured the resistivity of the superconducting core on a Physical Property Measurement System. The microstructure of the tape was analyzed by scanning electron microscopy (SEM, Zeiss SIGMA) . The magneto-optical (MO) image of the superconducting core was obtained using an optical cryostat (Montana Instruments) at Argonne National Laboratory. We polished the

superconducting core after tearing off the silver sheath on that side. A Bi-substituted iron-garnet indicator film was placed in direct contact with the superconducting core as a magnetic field sensor [22]. The magnetic field generated from a homemade copper coil is applied with the direction perpendicular to the tape surface.

Results and discussion

Fig. 1 shows the XRD pattern of the $CaKFe_4As_4$ precursor. We find that most of the diffraction peaks can be well indexed with the P4/mmm space group. There are additional reflections evidencing the presence of a small amount of residual Fe with Im-3m structure. However, we find no trace of KFe_2As_2 that is usually seen in the '1144' polycrystals. We thus perform Rietveld refinement with two phases. The refinement is successful as indicated by the reliability factors: R_p = 5%, R_{wp} =6.59%. The fitted lattice parameters are a=3.861 nm and b=12.830 nm. The calculated fractions of the $CaKFe_4As_4$ phase and the Fe phase are 97.2% and 2.8%, respectively. The EPMA measurements on 20 points of the superconducting core indicate that the average composition is $Ca_{0.97}K_{1.02}Fe_4As_4$, close to the nominal composition.

So far, scientists have found various stable 1144 systems with chemical formula $AeAFe_4As_4$, where Ae and A are the alkaline-earth and alkaline elements, respectively. The large difference between the radii of the Ae and the A ions is necessary for the formation of the 1144 structure [16] . Song et al further utilized density functional theory to study the stability of the 1144 system [23] and found that the P 4/mmm structure is sensitive to temperature. It is only stable below a critical temperature of T′~ 780 K (507 °C) . At higher temperatures, the 122 phase with I4/mmm structure will dominate. In order to obtain a comprehensive understanding of the phase stability during the post-annealing process, we perform TG analysis and DTA on the precursor. Fig. 2 shows the TG and DTA curves of the precursor under an argon atmosphere. The loss of the mass due to the evaporation of potassium is not as evident until the temperature is close to the melting temperature T_m~ 950 °C at which point there is a sharp endothermic peak. At intermediate temperature, there is a sharp exothermic peak at 522 °C as shown in the inset, which may be correlated with the critical temperature T′ predicted by the theoretical calculation.

In order to further verify this prediction, the $CaKFe_4As_4$ precursor is put in an alumina crucible, sealed in a silicon tube and reheated at 800 °C for 0.5 h which is much higher than the T′ . The precursor is then fast cooled to room temperature. However, the diffraction pattern of the precursor changes little after the reheating process, as shown in Fig. 3(a) and (b) , indicating that

the $CaKFe_4As_4$ phase is stable during the post-annealing process. Therefore, we anneal the $CaKFe_4As_4$ tapes at different temperatures for 0.5 h to optimize the sintering temperature. As shown in Fig. 3(c) , all the diffraction peaks of the tape annealed at 500 °C for 0.5 h can be well indexed with the P 4/mmm space group. There is no evidence for a secondary phase. One can see a great enhancement of the intensities of the (00l) peaks, suggesting a strong c -axis texture. In order to quantitatively evaluate the c -axis texture, we utilize the Lotgering method to calculate $F=(\rho-\rho_0)/(1-\rho_0)$ [24] , where $\rho = \sum I(00l) / \sum I(hkl)$, $\rho_0 = \sum I_0(00l) / \sum I_0(hkl)$. I and I_0 are the intensities of every peak for the textured and randomly oriented samples, respectively. The calculated F value for the Ca1144 tapes annealed at 500 C is 0.565, which is intermediate between the $Sr_{0.6}K_{0.4}Fe_2As_2$ superconducting tape [25] (F~0.476) and the $Ba_{0.6}K_{0.4}Fe_2As_2$ superconducting tape [26] (F~ 0.590) . The large F value of the $CaKFe_4As_4$ tape indicates that the cold working process including drawing and rolling can effectively align the grains with the c axis perpendicular to the tape surface. When the post-annealing temperature increases up to 700 °C, obvious minor phases appear in the diffraction pattern, namely the KFe_2As_2 and the CaAgAs phases, as shown in Fig. 3(d) . Moreover, sintering at 800 °C largely suppresses the intensity of the $CaKFe_4As_4$ diffraction peaks, making KFe_2As_2 the predominant phase. Based on the above XRD results, we suggest that the $CaKFe_4As_4$ phase reacts strongly with the silver sheath and produces KFe_2As_2 and CaAgAs at temperature above 500 °C. KFe2 As2 is a superconductor with Tc~ 3.5 K [27], while CaAgAs is a topological insulator [28] . The impurity phases deteriorate the superconductivity of the superconducting core and decrease the overall supercurrent. Therefore, different from the K-doped FeAs122 tapes which have a proper sintering temperature widow ranging from 700 °C to 900 °C, we suggest that the $CaKFe_4As_4$ tapes can only be post-annealed below 500 °C.

We measure the critical current of the CaKFe4 As4 tapes annealed at different temperatures. As expected, all the tapes sintered at 700 °C and 800 °C show no trace of supercurrents at 4.2 K. In contrast, we do observe a supercurrent in the tape post-annealed at 500 °C, as shown in Fig. 4. At 0 T, the transport J_c is 2.7×10^4 A cm^{-2} (critical current I_c~ 129 A) . With increasing field, the critical current density exhibits a strong field dependence and decreases to a value at 10 T that is nearly one-tenth of that at self-field. Furthermore, there is a clear hysteresis of Ic when the field decreases from 14 T, indicating a weak-link effect. The transport J_c at 4.2 K and 10 T is 2.2×10^3 A cm^{-2} . This value is one order of magnitude larger than the 1111 [29] and Co-doped 122 rolled tapes [30] , but much smaller than that of the K-doped 122 rolled tapes [3] .

The main panel of Fig. 5(a) shows the temperature dependence of normalized resistance at 0 T. The silver sheath is peeled off before the measurement. With decreasing temperature, the resistance exhibits a metallic like behavior and suddenly drops at $T_c \sim$ 35 K. The residual resistance ratio is RRR =ρ(300 K)/ρ(35 K)= 4.65, close to that of the hot pressed $Sr_{0.6}K_{0.4}Fe_2As_2$ tapes [31] . However, the superconducting transition width ΔTc∼ 5 K is rather large, which may be caused by bad connectivity. As shown in the insets of Fig. 5(a), the T_c^{onset} determined from the 90% criterion decreases very little with increasing field, while the T_c zero de fined with the 10% criterion is largely suppressed by the field, resulting in an obvious tail feature near Tc zero. Fig. 5(b) shows the B–T phase diagram. One can see the very steep temperature dependence of B_{c2} typically found in IBSs [32]. The slopes of the upper critical field, $-dB_{c2}/dT$, are 6.0 T K^{-1} and 9.7 T K^{-1} for the field perpendicular and parallel to the tape, respectively. These values are larger than that of the single crystal, but close to the value of the CaKFe4As4 powder sample [21]. The B_{c2} at 0 K determined with the Werthamer–Helfand–Hohenberg formula is 242 T and 110 T for the field parallel and perpendicular to the tape surface, respectively. The anisotropy parameter of B_{c2}, $\gamma = B_{c2}^{//}/B_{c2}^{\perp}$, is 2.32 near T_c and decreases to 1.86 at 33.4 K, as shown in the inset of Fig. 5(b).

The tail structure in the magnetoresistance curves may imply a possible thermal activated flux flow (TAFF) behavior. According to the TAFF model, the resistivity can be expressed as $\rho(T, H)=2\rho_c U\exp(-U/T)/T$, where U is the thermally activated energy or pinning potential. Assuming that $\rho_{0f} =2\rho_c U/T$ is a temperature independent constant, the thermal activation energy is $U=U_0(1-T/T_c)$, and we can obtain the Arrhenius relation:

$$\ln\rho(T,H)=\ln\rho_{0f}-U_0(H)/T+U_0(H)/T_c=\ln\rho_0-U_0(H)/T,$$

where $\ln\rho_0=\ln\rho_{0f}+U_0(H)/T_c$. The pinning potential can be evaluated from the slope, $U_0(H)=-d\ln\rho/d(1/T)$. We depict the field dependences of U_0 for the two field directions in Fig. 5(c) . The pinning potential at 0.5 T with the field perpendicular to the tape is 650 K. It is much smaller than the K-doped 122 single crystal and tape [13 , 33] , implying weak thermal barrier against vortex motion. The pinning potential shows a weak power-law field dependence, namely $U_0 \propto B^{-n}$, with n= 0.12 and 0.14 for field perpendicular and parallel to the tape surface, respectively, manifesting a small anisotropy.

Fig. 6(a) presents the optical image of the transverse section of the $CaKFe_4As_4$ tape showing a typical superconducting core with a saddle shape which arises due to the stronger deformation in the middle as compared to the two edges. Fig. 6(b) shows a SEM image of the

longitudinal section of the superconducting core. As a result of the low temperature sintering, the average size of the grains is as small as 2 μm. There are clearly observable voids and pores, limiting the actual current path along the tape. Fig. 6(c) shows a MO image of the $CaKFe_4As_4$ superconducting tape. MO images reveal the normal component of the magnetic induction, that is, the vortex density, at the imaged sample surface with a bright contrast representing high density. Note that in the current implementation this imaging technique does not distinguish between positive and negative vortices. The sample is cut into a rectangular shape with dimensions $4.08\times3.20\times0.18$ mm^3. We firstly cool the sample to 5 K in zero field. Then we increase the field to 82.7 mT and decrease it to zero to prepare the sample in the remanent state. We can see two bright areas corresponding to the thickest sections of the superconducting core which trap a high vortex density. The transverse feathering feature may be due to residual damage and cracking arising in the rolling process. The bright contrast along the center-line of the sample represents negative vortices which are generated by the return field from the vortices trapped in the thicker sample sections on either side. Based on the SEM and MO images, we suggest that bad connectivity between superconducting grains is responsible for the low J_c at high magnetic field.

Conclusions

In summary, we have fabricated Ag-sheathed $CaKFe_4As_4$ tapes by ex situ PIT method. We find that $CaKFe_4As_4$ strongly reacts with the silver sheath during the post-annealing process at temperature higher than 500 °C. Therefore, we sintered the tape at 500 °C and obtained a self-field J_c of $2.7\text{x}10^4$ A cm^{-2} at 4.2 K. The J_c exhibits a strong field dependence and decreases to $2.2\text{x}10^3$ A cm^{-2} at 10 T. Magneto-transport and MO imaging reveal weak-link effects in the tape. The pinning potential derived from the magnetoresistance measurement is one order of magnitude smaller than that of the $Ba_{1-x}K_xFe_2As_2$ tapes. Coupled with the SEM image, we conclude that the bad connectivity between the grains due to low temperature sintering is the main factor limiting the critical current at high magnetic field. Considering the inherent high critical current density in the $CaKFe_4As_4$ single crystal, the polycrystalline wires and tapes are still promising for practical application if we use a sheath material that is chemically inert to $CaKFe_4As_4$ at high temperature and apply a proper post-annealing process to improve the grain connectivity.

Acknowledgments

The authors would like to thank Dr Fang Liu and Professor Huajun Liu in the High Magnetic Field Laboratory of the Chinese Academy of Sciences. We also thank Chen Li for help and useful suggestions. This work is partly supported by the National Natural Science Foundation of China (grant no. 51320105015), the Beijing Municipal Science and Technology Commission (grant no. Z171100002017006), the Bureau of Frontier Sciences and Education, Chinese Academy of Sciences (QYZDJ-SSW-JSC026), the Bureau of International Cooperation, Chinese Academy of Sciences (182111KYSB20160014) and Strategic Priority Research Program of Chinese Academy of Sciences (grant no. XDB25000000). Magneto-optical work was carried out at Argonne National Laboratory and supported by the US Department of Energy, Office of Science, Materials Sciences and Engineering Division.

References

[1] Kamihara Y, Watanabe T, Hirano M and Hosono H 2008 Iron-Based Layered Superconductor $La[O_{1-x}F_x]FeAs$ (x = 0.05−0.12) with T_c = 26 K *J. Am. Chem. Soc.* **130** 3296–7

[2] Hosono H, Yamamoto A, Hiramatsu H and Ma Y 2018 Recent advances in iron-based superconductors toward applications *Mater. Today* **21** 278–302

[3] Dong C, Yao C, Lin H, Zhang X, Zhang Q, Wang D, Ma Y, Oguro H, Awaji S and Watanabe K 2015 High critical current density in textured Ba-122/Ag tapes fabricated by a scalable rolling process *Scr. Mater.* **99** 33–6

[4] Zhang X, Oguro H, Yao C, Dong C, Xu Z, Wang D, Awaji S, Watanabe K and Ma Y 2017 Superconducting Properties of 100-m Class $Sr_{0.6}K_{0.4}Fe_2As_2$ Tape and Pancake Coils *IEEE Trans. Appl. Supercond.* **27** 7300705

[5] Dong C, Yao C, Zhang X, Wang D and Ma Y 2018 Critical Current Density and Flux Pinning Mechanism in Flat-Rolled Sr-122/Ag Tapes *IEEE Trans. Appl. Supercond.* **28** 1–5

[6] Togano K, Gao Z, Matsumoto A and Kumakura H 2013 Enhancement in transport critical current density of ex situ PIT Ag/(Ba, K)Fe_2As_2 tapes achieved by applying a combined process of flat rolling and uniaxial pressing *Supercond. Sci. Technol.* **26** 115007

[7] Yao C, Lin H, Zhang X, DongliangWang, Zhang Q, Ma Y, Awaji S and Watanabe K 2013 Microstructure and transport critical current in $Sr_{0.6}K_{0.4}Fe_2As_2$ superconducting tapes prepared by cold pressing *Supercond. Sci. Technol.* **26** 075003

[8] Lin H, Yao C, Zhang X, Dong C, Zhang H, Wang D, Zhang Q, Ma Y, Awaji S, Watanabe K, Tian H and Li J 2014 Hot pressing to enhance the transport J_c of $Sr_{0.6}K_{0.4}Fe_2As_2$

superconducting tapes *Sci. Rep.* **4** 6944

[9] Weiss J D, Tarantini C, Jiang J, Kametani F, Polyanskii A A, Larbalestier D C and Hellstrom E E 2012 High intergrain critical current density in fine-grain $(Ba_{0.6}K_{0.4})Fe_2As_2$ wires and bulks *Nat. Mater.* **11** 682–5

[10] Liu S, Lin K, Yao C, Zhang X, Dong C, Wang D, Awaji S, Kumakura H and Ma Y 2017 Transport current density at temperatures up to 25 K of Cu/Ag composite sheathed 122-type tapes and wires *Supercond. Sci. Technol.* **30** 115007

[11] Pyon S, Suwa T, Park A, Kajitani H, Koizumi N, Tsuchiya Y, Awaji S, Watanabe K and Tamegai T 2016 Enhancement of critical current densities in $(Ba,K)Fe_2As_2$ wires and tapes using HIP technique *Supercond. Sci. Technol.* **29** 115002

[12] Gao Z, Togano K, Matsumoto A and Kumakura H 2015 High transport *J*c in magnetic fields up to 28 T of stainless steel/Ag double sheathed Ba122 tapes fabricated by scalable rolling process *Supercond. Sci. Technol.* **28** 012001

[13] Zhang X, Yao C, Lin H, Cai Y, Chen Z, Li J, Dong C, Zhang Q, Wang D, Ma Y, Oguro H, Awaji S and Watanabe K 2014 Realization of practical level current densities in $Sr_{0.6}K_{0.4}Fe_2As_2$ tape conductors for high-field applications *Appl. Phys. Lett.* **104** 202601

[14] Yeoh W K, Gault B, Cui X Y, Zhu C, Moody M P, Li L, Zheng R K, Li W X, Wang X L, Dou S X, Sun G L, Lin C T and Ringer S P 2011 Direct Observation of Local Potassium Variation and Its Correlation to Electronic Inhomogeneity in $(Ba_{1-x}K_x)Fe_2As_2$ Pnictide *Phys. Rev. Lett.* **106** 247002

[15] Dong C, Yao C, Huang H, Zhang X, Wang D and Ma Y 2017 Calorimetric evidence for enhancement of homogeneity in high performance $Sr_{1-x}K_xFe_2As_2$ superconductors *Scr. Mater.* **138** 114–9

[16] Iyo A, Kawashima K, Kinjo T, Nishio T, Ishida S, Fujihisa H, Gotoh Y, Kihou K, Eisaki H and Yoshida Y 2016 New-Structure-Type Fe-Based Superconductors: $CaAFe_4As_4$ (A = K, Rb, Cs) and $SrAFe_4As_4$ (A = Rb, Cs) *J. Am. Chem. Soc.* **138** 3410–5

[17] Meier W R, Kong T, Kaluarachchi U S, Taufour V, Jo N H, Drachuck G, Ohmer A E B, Saunders S M, Sapkota A, Kreyssig A, Tanatar M A, Prozorov R, Goldman A I, Balakirev F F, Gurevich A, Ko S L B and Canfield P C 2016 Anisotropic thermodynamic and transport properties of single-crystalline $CaKFe_4As_4$ *Phys. Rev. B* **94** 064501

[18] Meier W R, Kong T, Bud'ko S L and Canfield P C 2017 Optimization of the crystal growth of the superconductor CaKFe4As4 from solution in the FeAs−CaFe2As2−KFe2As2 system Phys. Rev. Mater. 1 013401

[19] Cho K et al 2017 Nodeless multiband superconductivity in stoichiometric single-crystalline CaKFe4As4 Phys. Rev. B 95 100502

[20] Mishev V, Nakajima M, Eisaki H and Eisterer M 2016 Effects of introducing isotropic artificial defects on the superconducting properties of differently doped Ba-122 based single crystals Sci. Rep. 6 27783

[21] Singh S J, Bristow M, Meier W R, Taylor P, Blundell S J, Canfield P C and Coldea A I 2018 Ultrahigh critical current densities, the vortex phase diagram, and the effect of granularity of the stoichiometric high-Tc superconductor $CaKFe_4As_4$ *Phys Rev Mater.* **2** 074802

[22] Vlasko-Vlasov V K, Crabtree G W, Welp U and Nikitenko V I 1999 Magneto-optical studies of magnetization processes in high-Tc superconductors, Physics and Materials Science of Vortex States, Flux Pinning and Dynamics (Nato Advanced Science Institutes Series, Series E, Applied Sciences vol 356) ed R Kossowsky et al pp 205–37

[23] Song B Q, Nguyen M C, Wang C Z and Ho K M 2018 Stability of the 1144 phase in iron pnictides Phys. Rev. B 97 094105

[24] Lotgering F K 1959 Topotactical reactions with ferrimagnetic oxides having hexagonal crystal structures: I J. Inorg. Nucl. Chem. 9 113–23

[25] Huang H, Yao C, Zhu Y, Zhang X, Dong C, Wang D, Liu S, Cheng Z, Awaji S and Ma Y 2018 Influences of tape thickness on the properties of Ag-sheathed Sr1−xKxFe2As2 superconducting tapes IEEE Trans. Appl. Supercond. 28 6900105

[26] Cheng Z, Zhang X, Yao C, Dong C, Wang D, Huang H, Liu S and Ma Y 2018 Effect of wire diameter on the microstructure and Jc properties of Ba0.6K0.4Fe2As2 tapes IEEE Trans. Appl. Supercond. 28 7300505

[27] Liu Y, Tanatar M A, Kogan V G, Kim H, Lograsso T A and Prozorov R 2013 Upper critical field of high-quality single crystals of KFe2As2 Phys. Rev. B 87 477

[28] Nayak J, Kumar N, Wu S-C, Shekhar C, Fink J, Rienks E D L, Fecher G H, Sun Y and Felser C 2018 Electronic properties of topological insulator candidate CaAgAs J. Phys.: Condens. Matter 30 045501

[29] Zhang Q, Zhang X, Yao C, Huang H, Wang D, Dong C, Ma Y, Ogino H and Awaji S 2017 Enhanced transport critical current density in Sn-added SmFeAsO1−xFx tapes prepared by the PIT method Supercond. Sci. Technol. 30 065004

[30] Dong C, Yao C, Huang H, Wang D, Zhang X and Ma Y 2017 Superconducting properties of PIT BaFe2-xCoxAs2 tapes IEEE Trans. Appl. Supercond. 27 7300204

[31] Dong C, Lin H, Huang H, Yao C, Zhang X, Wang D, Zhang Q, Ma Y, Awaji S and Watanabe K 2016 Vortex pinning and dynamics in high performance Sr0.6K0.4Fe2As2 superconductor J. Appl. Phys. 119 143906

[32] Gurevich A 2011 To use or not to use cool superconductors? Nat. Mater. 10 255–9

[33] Wang X-L et al 2010 Very strong intrinsic flux pinning and vortex avalanches in (Ba, K)Fe2As2 superconducting single crystals Phys. Rev. B 82 024525

Figures

Fig.1. Powder XRD pattern and Rietveld refinement of the $CaKFe_4As_4$ precursor.

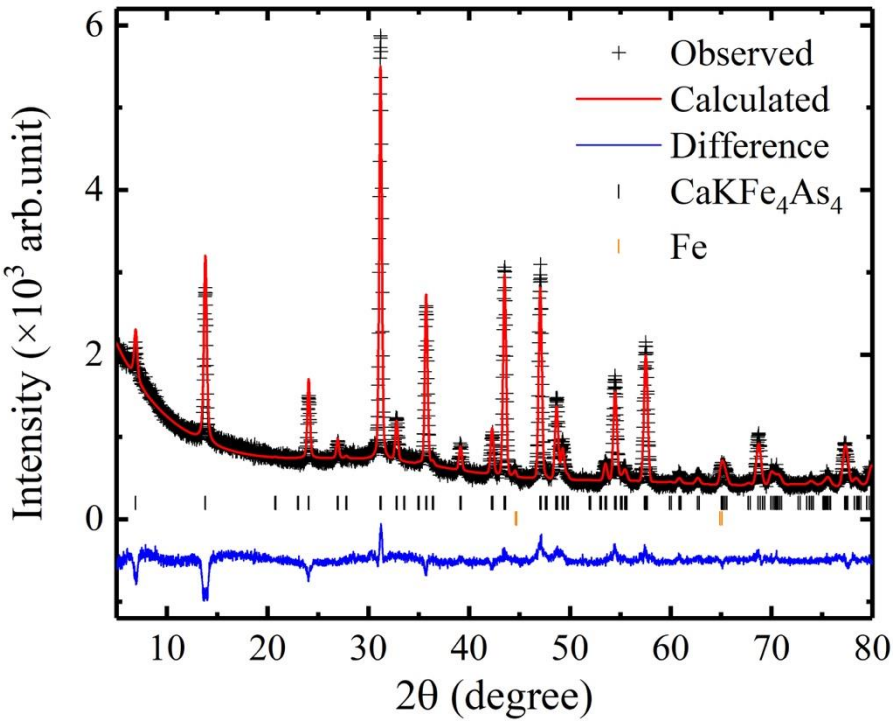

Fig. 2. TG and DTA curves of the CaKFe4As4 precursor. The inset is the enlarged view of the DTA curve near 522 °C.

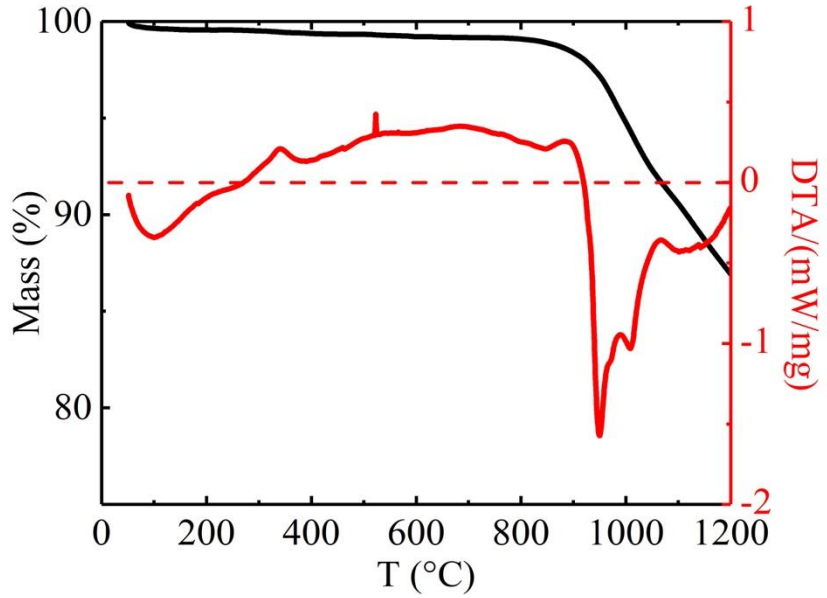

Fig. 3. XRD patterns of (a) the as-sintered $CaKFe_4As_4$ precursors, (b) the $CaKFe_4As_4$ precursors reheated at 800 °C for 0.5 h, and the $CaKFe_4As_4$ tapes sintered at (c) 500 °C, (d) 700 °C and (e) 800 °C for 0.5 h

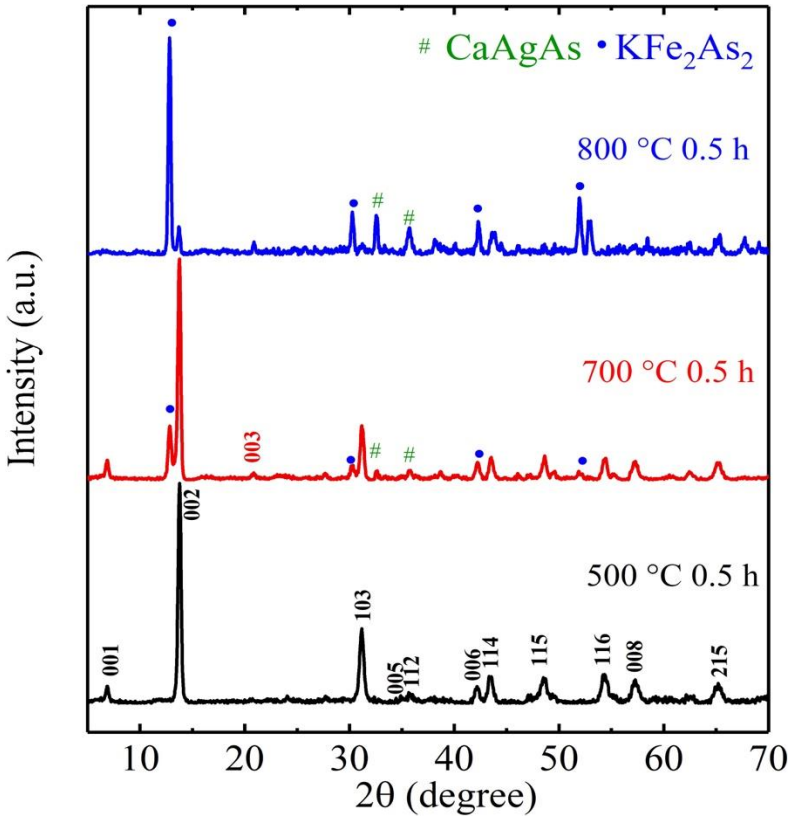

Fig.4. Magnetic field dependence of the transport J_c at 4.2 K with increasing and decreasing field for the $CaKFe_4As_4$ tapes sintered at 500 °C for 0.5 h.

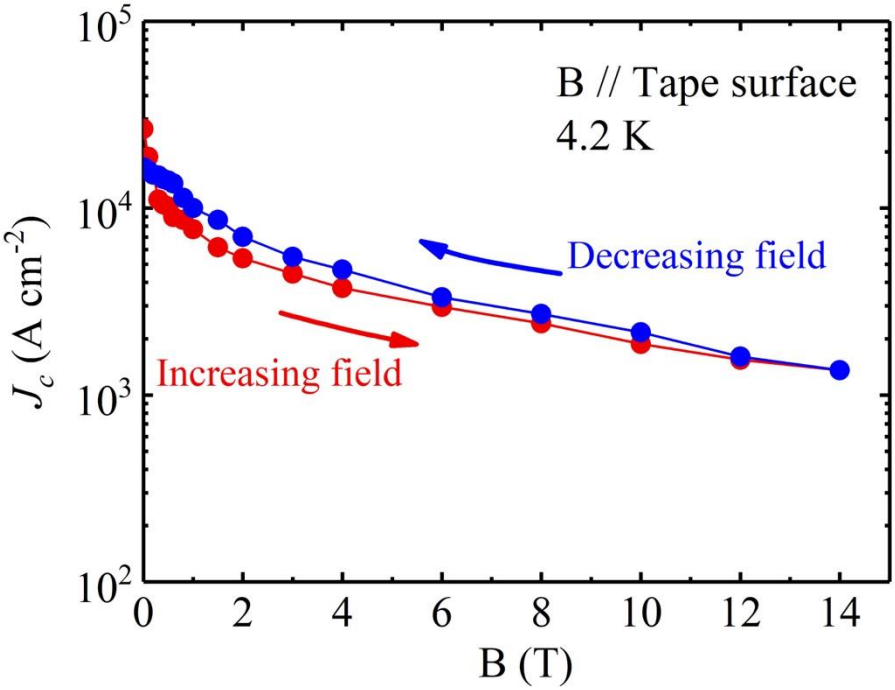

Fig.5. (a) Temperature dependence of normalized resistance for the $CaKFe_4As_4$ tapes. The inset shows the magnetoresistance near T_c with $H \perp$ tape and $H \parallel$ tape. (b) B-T phase diagram, the inset is the anisotropy parameter as a function of temperature. (c) Field dependences of pinning potential for $H \perp$ tape and $H \parallel$ tape.

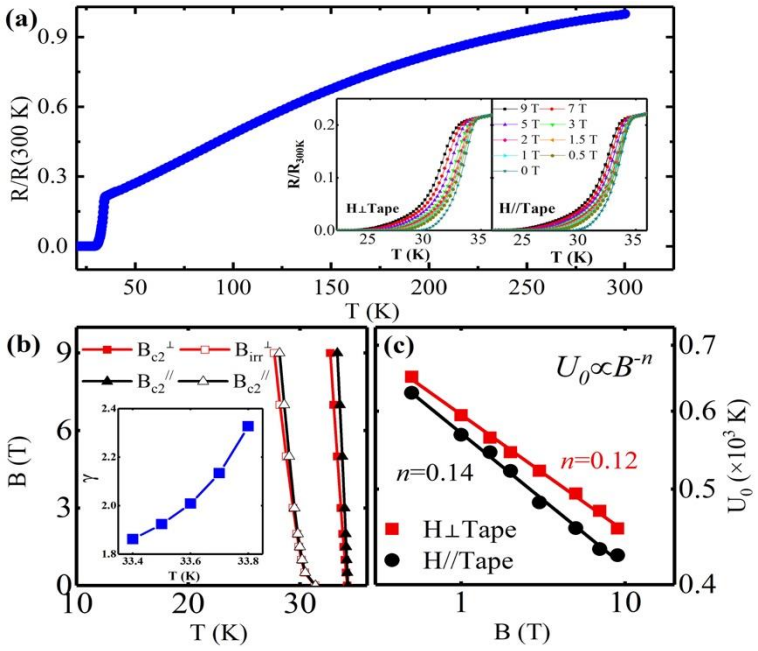
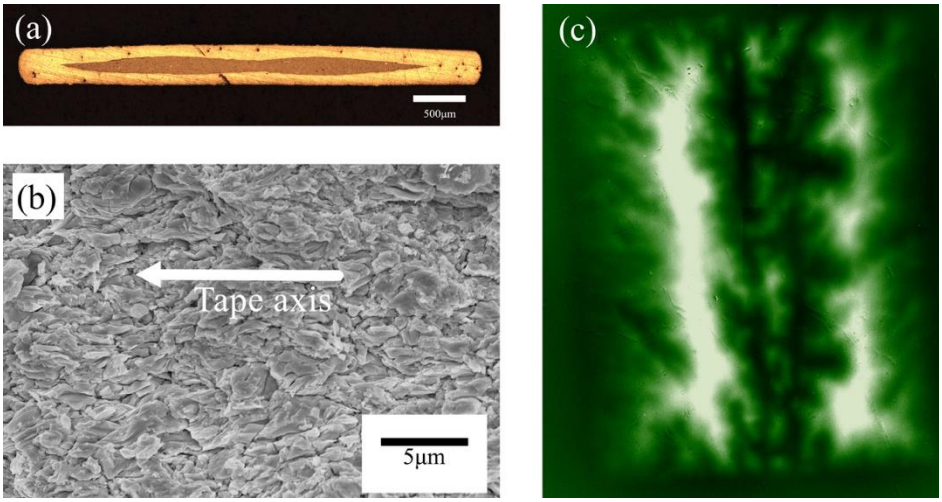
Fig. 6. (a) Optical image of the transverse cross-section of the $CaKFe_4As_4$ tapes. (b) SEM image of the longitudinal section of the superconducting core. (c) MO image of the superconducting core. In this image the tape axis is vertical.